

# Hemispherical emissivity of V, Nb, Ta, Mo, and W from 300 to 1000 K

S. X. Cheng,\* P. Cebe,† L. M. Hanssen, D. M. Riffe, and A. J. Sievers

Laboratory of Atomic and Solid State Physics and Materials Science Center, Cornell University, Ithaca, New York 14853-2501

Received September 2, 1986; accepted November 3, 1986

The hemispherical emissivities of five transition elements, V, Nb, Ta, Mo, and W, have been measured from 300 to 1000 K, complementing earlier higher-temperature results. These low-temperature data, which are similar, are fitted to a Drude model in which the room-temperature parameters have been obtained from optical measurements and the temperature dependence of the dc resistivity is used as input to calculate the temperature dependence of the emissivity. A frequency-dependent free-carrier relaxation rate is found to have a similar magnitude for all these elements. For temperatures larger than 1200 K the calculated emissivity is always greater than the measured value, indicating that the high-temperature interband features of transition elements are much weaker than those determined from room-temperature measurements.

## 1. INTRODUCTION

In 1978 it was shown that the high-temperature thermal emissivity of a good conductor such as Al and Cu could be modeled quite precisely by including the Holstein process of surface-assisted scattering into the Drude free-electron model.<sup>1</sup> Because the centroid of the blackbody spectrum,  $\langle\omega\rangle$ , is proportional to temperature and the electron-phonon scattering time  $\tau$  is inversely proportional to temperature, then for specular surface scattering the product  $\langle\omega\rangle\tau$  is a constant that is independent of temperature. For good conductors  $\langle\omega\rangle\tau > 1$  (Mott-Zener regime), and the temperature dependence of the normal and hemispherical emissivities,  $\epsilon_N(T)$  and  $\epsilon_H(T)$  respectively, is described by simple expressions<sup>2</sup> that involve both the dc resistivity  $\rho$  and the free-carrier density  $n$ , namely,

$$\epsilon_N(T) = \rho(T)\omega_p/2\pi + 3v_F/4c \quad (1)$$

and

$$\epsilon_H(T) = 4\epsilon_N(T)/3. \quad (2)$$

The first term in Eq. (1) is from phonon scattering, and the second is from diffuse surface scattering. For free electrons the plasma frequency  $\omega_p$  and the Fermi velocity  $v_F$  are determined from  $n$ .

In the Hagen-Rubens regime, where  $\langle\omega\rangle\tau \ll 1$ , Davisson and Weeks<sup>3</sup> showed that the hemispherical emissivity is a function only of  $\rho(T)$  and the temperature  $T$ . The resultant equation,

$$\begin{aligned} \epsilon_H = & 0.766(\rho T)^{1/2} - [0.309 - 0.0889 \ln(\rho T)](\rho T) \\ & - 0.0175(\rho T)^{3/2}, \end{aligned} \quad (3)$$

has been used to fit the data for alloys and also for some of the transition elements.<sup>4</sup> Although early studies<sup>5</sup> showed good agreement between Eq. (3) and the data for Pt, recent measurements on W that had been prepared in ultrahigh-vacuum (UHV) conditions have demonstrated that Eq. (3) is a poor approximation for this element<sup>6,7</sup> in the measured

temperature range from 340 to 1260 K. It is fair to ask how the temperature-dependent emissivity of these two transition elements can be different when the room-temperature resistivities differ only by a factor of 2. A related question is: Why should a normal skin-effect calculation [Eq. (3)] work at all for Pt at room temperature since the condition  $\langle\omega\rangle\tau \ll 1$  is not satisfied? The fact that an explanation of the difference between the two transition metals, Pt and W, has not been forthcoming indicates the level of understanding of the hemispherical emissivity of these metals.

In order to investigate the systematics of the temperature-dependent infrared properties of transition elements, we have made hemispherical emissivity measurements on single crystals of body-centered cubic elements from two columns of the periodic table. They are V, Nb, and Ta from column VB and Mo and W from column VIB. The  $\epsilon_H$  values for W in high vacuum (HV) obtained both with electron (e) -beam and radio-frequency (rf) sample heating are the same but are about 8% larger than the UHV data<sup>6,7</sup> over the entire temperature range. In this temperature regime these five elements are characterized by a large frequency-dependent contribution to the scattering time, indicative of two-conduction-band-like behavior. We propose that this frequency-dependent relaxation rate, which continues to grow with increasing energy until about 0.7 eV, provides the process whereby  $\langle\omega\rangle\tau$  can decrease with increasing temperature. Although the exact mechanism behind this scattering in transition elements has not been identified, the end result is that for elevated temperatures the optical resistivity at the blackbody centroid is larger than the dc value but smaller than calculated from the room-temperature optical parameters.

In the next section the transient calorimetric measuring system and experimental results are presented. Section 3 describes in detail how the emissivity data in the 300- to 1000-K region are fitted with a single-band model. Finally, in Section 4 our results for W are combined with earlier higher-temperature measurements to test the room-temperature optical parameters over a large temperature range.

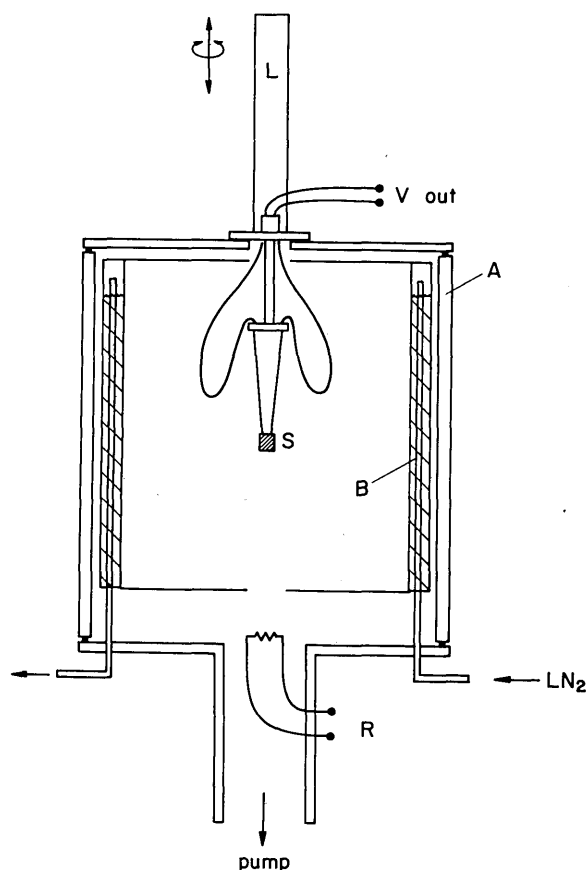


Fig. 1. Transient calorimetric vacuum system. The aluminum vacuum chamber A is attached to the 10.16-cm-diameter diffusion pump. The sample S, which is suspended from two 3-mil thermocouple wires, is surrounded by a liquid-N<sub>2</sub>-cooled chamber B, which is supported by its three thin-wall stainless-steel fill and exhaust tubes. Sample heating is obtained by translating the sample, which is attached to the vacuum manipulator L, through the cold shield down to the e-beam filament or the rf coil R.

The conclusions about interband transitions in high-temperature transition elements follow.

## 2. EXPERIMENTAL APPARATUS AND RESULTS

The transient calorimetric system used for these measurements is shown schematically in Fig. 1. The vacuum chamber (A) consists of a cylindrical chamber 20 cm in diameter and 28 cm in length surrounding an internal cold chamber 14 cm in diameter and 17 cm in length. A 10.16-cm-diameter oil-diffusion pump provides a base pressure of  $\sim 5 \times 10^{-7}$  Torr. The improvements over an earlier HV design<sup>8</sup> are fourfold: (1) A linear-rotary motion vacuum manipulator has been incorporated for rapid and precise adjustment of the sample height and to eliminate O-ring air leaks during sample translation, (2) a N<sub>2</sub> cold shroud encompasses most of the sample compartment, which permits measurements down to 300 K, (3) the data are continuously acquired, digitized, and stored in a computer for ease in later manipulation, and (4) an interchangeable sample heating assembly permits both e-beam and rf heating to be employed. The different components of the calorimeter are labeled in the caption for Fig. 1.

The samples are cut from single-crystal ingots in the shape of a thin disk or plate with the (100) face parallel to the large area surfaces ( $\sim 2$  cm<sup>2</sup>), then mechanically and electrically polished to optical quality, and finally spot welded to a pair of 3-mil-diameter WRe3%/WRe25% (or Chromel/Constantan) thermocouple wires. These in turn are suspended from an alumina insulating rod attached to the manipulator with the free ends passing under a stationary O-ring seal at an electrical feedthrough. Outside the chamber the thermocouple wires pass through a switch that allows the sample to be grounded, connected to a voltmeter, or maintained at high voltage when it is to be e-beam heated.

The procedure used in each data run consists of lowering the sample out of the liquid-N<sub>2</sub>-cooled chamber and positioning it about 1.3 cm above a Ta filament for e-beam heating (or inserting it into a water-cooled Cu coil for rf heating). After heating, the thermocouple leads are connected through the switch to a nanovoltmeter, and the output voltage with respect to the reference ice bath is fed into a digital multimeter. At the same time the sample is mechanically translated up into the center of the cold chamber. The multimeter is monitored by an 8080A microprocessor, which sends the data to a computer. A data-taking run, which consists of measuring the thermocouple voltage versus time, is initiated and controlled by this computer. The data-analysis procedure described in Ref. 6 has been programmed into the computer so that the output is the hemispherical emissivity as a function of temperature.

The experimental results for the hemispherical emissivity of Ta and W are shown in Fig. 2, and those for V, Nb, and Mo in Fig. 3. The open circles represent data taken with e-beam heating, and the crosses those with rf heating. It should be

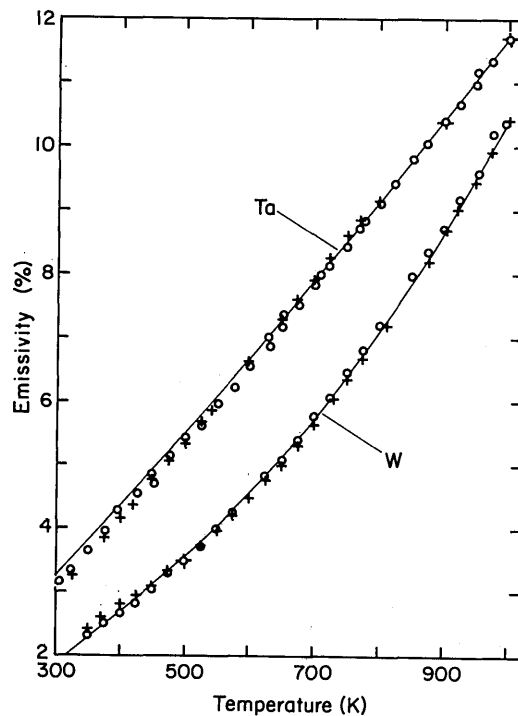


Fig. 2. Temperature dependence of the hemispherical emissivity of Ta and W. The open circles represent data taken with e-beam heating and the crosses those with rf heating of the sample. The solid curves represent the theoretical fit using the parameters given in Table 1.

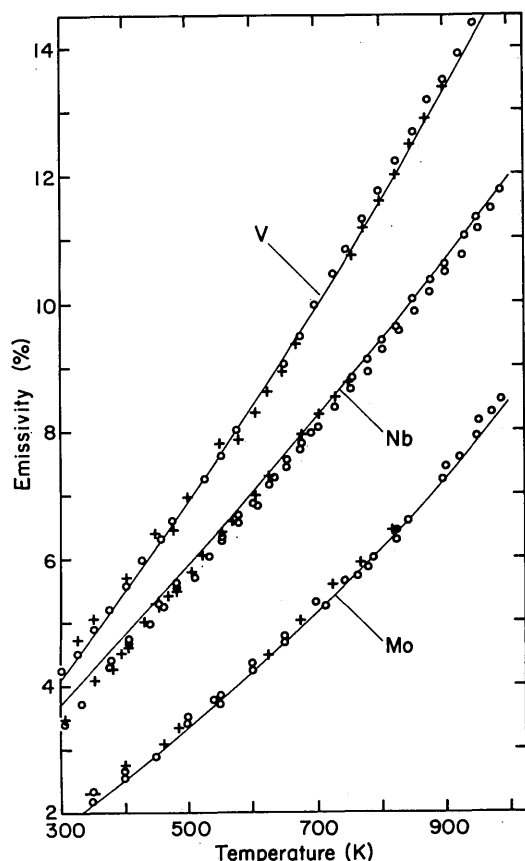


Fig. 3. Temperature dependence of the hemispherical emissivity of V, Nb, and Mo. The open circles represent data taken with e-beam heating and the crosses those with rf heating of the sample. The solid curves represent the theoretical fit using the parameters given in Table 1.

mentioned that this good agreement between these two heating methods occurs only when the first e-beam heating run of a series is used. One serious problem with e-beam heating has to do with the cleanliness of the vacuum pumping system itself. Use of an oil-based diffusion pump ensures that the some pump-oil vapor will appear in the vacuum chamber, and during e-beam heating this combination gives rise to the deposition of a thin C film on the sample. It has been identified by an electron microscope examination of the surface in the energy-dispersive mode. The thickness of this film increases with each heating cycle, causing a slight increase in the emissivity from run to run. No such degradation in the emissivity is found after repeated rf sample heating cycles.

### 3. COMPARISON OF THEORY AND EXPERIMENT

It has already been proposed<sup>1</sup> that the temperature dependence of the hemispherical emissivity be decomposed into its components to identify the different physical processes contributing to the high-temperature electron scattering time, and this possibility is now explored with this series of elements. We start with the known room-temperature optical properties. Since the infrared behavior of the room-temperature dielectric function for transition elements can be characterized with Drude model parameters,<sup>9</sup> it is expect-

ed that a similar characterization should be valid at elevated temperatures. With the dielectric function defined as

$$\epsilon(\omega) = \epsilon_1(\omega) + i\epsilon_2(\omega), \quad (4)$$

the real and imaginary parts to be used in the emissivity calculation are

$$\epsilon_1(\omega) = \epsilon_0 - \omega_p^2 \tau^2 / (1 + \omega^2 \tau^2), \quad (5)$$

$$\epsilon_2(\omega) = \epsilon_0 - \epsilon_1(\omega) / \omega \tau, \quad (6)$$

where  $\epsilon_0$  represents the low-frequency contribution from the high-frequency interband transitions, which are assumed to be outside the thermal spectral region. For the visible and the near IR at room temperature,  $\omega \tau \gg 1$ , so Eq. (5) simplifies to

$$\epsilon_1(\omega) = \epsilon_0 - \omega_p^2 / \omega^2. \quad (7)$$

The two model parameters,  $\epsilon_0$  and  $\omega_p$ , obtained by fitting Eq. (7) to the optical data<sup>10</sup> are given in Table 1. From  $\omega_p$ , the radius of the free-electron sphere normalized to the Bohr radius,  $r_s/a_0$ , also is obtained; it is presented in column 3 of the table. In the emissivity calculation these parameters are assumed to be temperature independent. Only a small change in  $\omega_p$  due to thermal expansion is expected. With  $\omega_p$  known, the dc resistivity  $\rho(T)$  gives the value of  $\tau(T)$  that can be substituted into Eqs. (5) and (6) to determine completely the temperature-dependent dielectric function and hence the surface impedance  $Z/Z_0$  since

$$Z/Z_0 = [\epsilon(\omega)]^{-1/2}. \quad (8)$$

The emissivity expressions are given by Eqs. (49) and (50) of Ref. 1.

This  $\tau(T)$  only gives a measure of the phonon-scattering contribution to the relaxation time. When  $\omega \tau > 1$  it is known that the Drude electrons are scattered in three ways: by the phonons  $\tau_\phi(T)$ , by the surface  $\tau_s$ , and by other electrons  $\tau_{ee}(T, \omega)$ . Because of the Holstein process of spontaneous phonon emission,  $\tau_\phi(T)$  is slightly smaller than  $\tau(T)$  when the temperature is comparable with the Debye temperature  $\theta_D$  [see Eq. (39) of Ref. 1]. The resultant relaxation frequency is obtained by adding these three relaxation-frequency components together; hence

$$1/\tau(T, \omega) = 1/\tau_\phi(T) + 1/\tau_s + 1/\tau_{ee}(T, \omega). \quad (9)$$

For the transition elements a two-conduction-carrier Drude model is often used to describe the dc conductivity.

Table 1. Drude Model Parameters<sup>a</sup>

Sample	$\omega_p$ (eV)	$r_s/a_0$	$\epsilon_0$	$f$	$p$	$\langle \omega \rangle \tau$ at 300 K
V	4.9	4.50	10.7	40	1.0	1.2
Nb	7.2	3.49	14.5	76	1.0	0.8
Ta	7.2	3.49	13.6	70	1.0	0.9
Mo	7.2	3.49	26.0	50	0.8	1.6
W	6.2	3.86	42.0	47	0.3	2
W <sup>b</sup>	7.0	3.55	42.0	69	0.6	1.7

<sup>a</sup> The parameters are determined from the room-temperature optical dielectric function and from the temperature dependence of the hemispherical emissivity between 300 and 1000 K. These parameters are defined in the text.

<sup>b</sup> Ref. 13.

Hopfield<sup>11</sup> has shown that if (now labeling the two carriers *a* and *b*)  $\omega\tau_a \gg 1$  and  $\omega\tau_b \ll 1$  or if  $\omega\tau_a > 1$ ,  $\omega\tau_b < 1$ , and  $(2\omega_{pb}^2/\omega_{pa}^2)\omega^2\tau_b^2 \ll 1$ , then the effective relaxation frequency is<sup>12</sup>

$$(1/\tau)_{\text{eff}} \approx 1/\tau_a + (\omega_{pb}^2/\omega_{pa}^2)\tau_b\omega^2. \quad (10)$$

This scattering time has exactly the same initial frequency dependence as given by  $1/\tau_{ee}$  in Eq. (9). Although only a single-carrier model is used in our analysis, by permitting the scattering time to have a frequency dependence of the  $1/\tau_{ee}$  form a key feature of the two-band model is automatically included.

When the optical data and  $\rho_{dc}$  are employed, only two adjustable parameters remain in Eq. (9): *f*, in

$$1/\tau_{ee}(T, \omega) = f\omega_p[(k_B T/\hbar\omega_p)^2 + (\omega/2\pi\omega_p)^2], \quad (11)$$

and *p*, in

$$1/\tau_s = (1-p)3\omega_p v_F/8c, \quad (12)$$

where *p*, the surface specularity parameter,<sup>13</sup> can range only between 0 and 1. These two parameters play important roles in the determination of  $\epsilon_H(T)$  in different temperature regimes: the value for *p* comes from the low-temperature data and the value for *f* from the high-temperature results. The fitted values are given in Table 1.

Inspection of columns 5 and 6 of Table 1 shows that all these elements have a large frequency-dependent scattering term and that three show specular scattering at the surface. The sign of the discrepancy between the model and the results at the lowest temperatures for Ta in Fig. 2 and Nb in Fig. 3 indicates that the plasma frequencies obtained from the room-temperature optical data for these elements are a bit too large. Two sets of data are given for W in Table 1: the fifth row uses the  $\omega_p$  determined from the optical data, while the sixth uses the  $\omega_p$  value determined with a new IR interferometric method.<sup>14</sup> The large differences in the *f* and *p* values in these two rows stem directly from the different  $\omega_p$  values and give some measure of the systematic errors associated with these results. Since the interferometrically determined value of  $\omega_p$  is available only for W, one should expect similar uncertainties in the values obtained for the different elements. No fundamental information can be extracted from the *p* values since in HV the surfaces are coated with adsorbed gases and adsorbates on clean surfaces<sup>7</sup> change  $\epsilon_H(T)$  by a few percent. At high temperatures  $1/\tau_{ee}(T, \omega)$  is comparable with  $1/\tau_\phi(T)$ , so small changes in  $\epsilon_H(T)$  produced by adsorbates translate into small changes in the *f* values. The *f* values in Table 1 are  $\sim 100$  times larger than the corresponding value<sup>15</sup> for Ag.

#### 4. DISCUSSION AND CONCLUSIONS

The qualitative behavior of the emissivity for all these elements is the same: with increasing temperature  $\epsilon_H(T)$  is concave upward, with the curvature consistently smaller for the periodic table column VB elements. Note that Eq. (3) can only give concave downward behavior. A more quantitative assessment of the data has been made with a numerical calculation of  $\epsilon_H(T)$  for a Drude metal. With  $\omega_p$  and  $\epsilon_0$  determined from published data<sup>10</sup> on the room-temperature IR dielectric function, the electron-electron scattering coefficient *f* has been determined. It is reasonable to expect

that this determination of *f* from the temperature dependence of  $\epsilon_H$  between 300 and 1000 K should permit  $\epsilon_H$  to be predicted for these transition elements at even larger temperatures. From the measured temperature dependence of the dc resistivity,  $\epsilon_H(T)$  can be calculated without any additional fitting parameters, and these values should provide a lower limit for the emissivity since the direct excitation of low-lying interband transitions has not been included in the surface impedance calculation of the metal surface. Besides this intrinsic process, extrinsic processes such as surface roughness and oxide coatings will provide additional contributions to  $\epsilon_H$  that have been ignored. Hence if the low-temperature model is still accurate at high temperatures then the measured emissivity can never be smaller than this calculated value.

To see how close the minimum allowed theoretical emissivity is to the measured one, a comparison has been made for the one element, W, for which the temperature dependence of the resistivity has been measured<sup>16</sup> up to 3600 K. Figure 4 shows both the measured and calculated emissivities over this entire temperature range. The low-temperature data (solid curve,  $T \leq 1100$  K) are from the earlier UHV work,<sup>6</sup> and the high-temperature data (solid curve,  $T \geq 1100$  K) are from Parker and Abbott.<sup>4</sup> Dotted-dashed curve *c* is obtained with the parameters listed in the caption, which are similar to those used in the low-temperature fit given in Table 1. The poor agreement at high temperature between theory and experiment deserves further examination, especially since the theory curve is above the experimental one.

To illustrate the relative importance of the different contributions to  $\epsilon_H$  at high temperatures, calculations have been carried out with  $\hbar\omega_p = 7$  eV and the other parameters varied in succession. They are identified in Fig 4 by the following dotted-dashed curves: *a*, the Drude model with specular scattering ( $\epsilon_0 = 1$ ,  $f = 0$ ,  $p = 1$ ); *b*, with the low-frequency part of the interband transitions included ( $\epsilon_0 = 42$ ,  $f = 0$ ,  $p =$

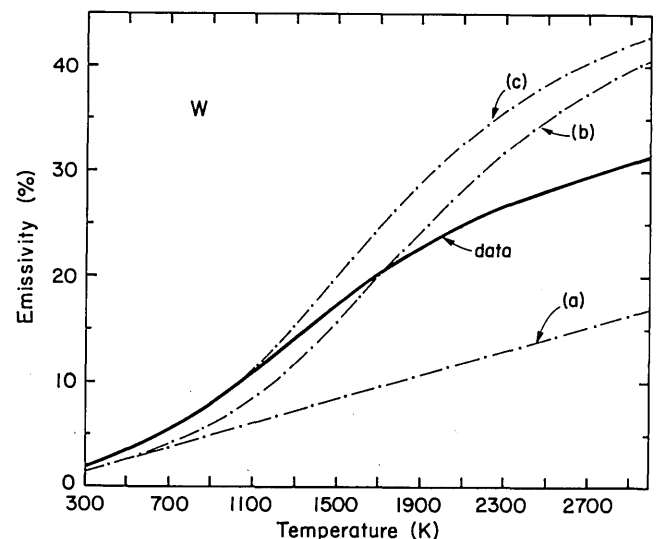


Fig. 4. Comparison of the model and hemispherical emissivity data of W from 300 to 3000 K. The experimental results are represented by the solid line: the data below 1100 K are from Ref. 6 and the data above that temperature from Ref. 4. Curve *a*, the Drude model with  $\epsilon_0 = 1$ ,  $f = 0$ , and  $p = 1$ . Curve *b*, low-frequency part of interband included with  $\epsilon_0 = 42$ ,  $f = 0$ , and  $p = 1$ . Curve *c*, strong electron-electron or two-band scattering with  $\epsilon_0 = 42$ ,  $f = 50$ , and  $p = 1$ . These parameters are defined in the text.

1); and c, strong electron–electron or two-band scattering ( $\epsilon_0 = 42, f = 50, p = 1$ ). Curve a provides an absolute lower limit since it counts only the Drude electrons, but it is far below the experimental data in Fig. 4. The interband term provides the major correction to the simple free-electron picture for calculating  $\epsilon_H$  at elevated temperatures, but the functional dependence does not follow the experimental data. Curve b overestimates  $\epsilon_H$  at 3000 K because the centroid frequency of the blackbody spectrum is large enough to correspond to the frequency where the real part of the dielectric function goes to zero; hence the underlying assumption of the model (that the thermal energies are small compared with the interband energies) is violated. Putting this assumption aside for the moment, we note that since the experimental values are less than these calculated values, most of the interband strength must actually occur at energies much larger than the thermal energies encountered here. Since the position of this zero is fixed by fitting the room-temperature IR dielectric function ( $\epsilon_0 = 42$ ), at these high temperatures the appropriate value of  $\epsilon_0 \ll 42$ . Adding the electron–electron or two-band contribution, curve c, produces good agreement with experiment at low temperatures but only aggravates the high-temperature discrepancy.

By fitting the measured room-temperature optical dielectric function in the 1-eV region with a parameterized dielectric function and then calculating  $\epsilon_H(T)$ , one can probe the temperature dependence of the interband transitions. We have done this and found that at high temperatures the calculated curve is larger than the experimental one, similar to curve c of Fig. 4, illustrating that the high-temperature optical interband features must be much weaker than those obtained from room-temperature measurements.

A common missing ingredient in all calculated fits to  $\epsilon_H(T)$  in Fig. 4 is the knee in the experimental data at about 2000 K. Above this temperature the  $\epsilon_H(T)$  dependence has a slope similar to that given from the dc resistivity (curve a). A similar shape is found in the experimental  $\epsilon_H(T)$  data for Nb and Ta.<sup>4</sup> These results indicate that the room-temperature interband transitions may not play the key role with regard to the high-temperature emissive properties of these elements. Fits with  $\epsilon_0 = 1$  appear to have the correct temperature dependence at high temperatures, but the magnitude is too small. We conclude that the standard Drude model, which correctly accounts for the room-temperature dielectric function, does not have temperature-independent coefficients; hence these parameters cannot be used to predict the high-temperature emissive properties.

The two-conduction-band picture provides another way to model the high-temperature dielectric function. At least qualitatively, this model gives the correct overall behavior: at low temperatures the emissivity is controlled by  $1/\tau_a$ ; in the 300- to 1000-K region the effective scattering rate shows a quadratic frequency dependence, while at high temperatures a constant relaxation frequency ( $\omega_{pb}^2/\tau_b\omega_{pa}^2$ ) provides the additional contribution. A more quantitative comparison shows that if this second contribution is temperature independent then the high-temperature behavior in Fig. 4 could be obtained, but only at nonphysical temperatures much larger than 3000 K. The effective frequency-dependent scattering rate approaches its high-frequency asymptote much too slowly to reproduce the knee in the emissivity data.

Since high-temperature IR spectroscopic measurements have not been made on the transition elements, the exact source of the spectroscopic feature at 0.68 eV that produces the knee in the W emissivity results cannot yet be made with certainty. Whatever the source, the absence of an identifiable feature at this energy in the optical properties at room temperature<sup>10</sup> indicates that this process must have an unusual temperature dependence.

The explanation of the good agreement between the Davisson–Weeks calculated result for  $\epsilon_H$  and the experimental data for Pt is now clear. The Davisson–Weeks limit of  $\epsilon_H(\rho_{dc}, T)$  overestimates the correct value because even at high temperature Pt is not in the Hagen–Rubens regime (since  $\langle\omega\rangle\langle 1/\tau\rangle^{-1} \approx 1$ ); however, this overestimate is sufficient to put the calculated value close to the experimentally measured one. Our measurements show that at elevated temperatures two-band-like scattering becomes important in five transition elements. The similarity of our results leads us to propose that the same effect occurs in Pt as well. Although the exact mechanism behind the scattering in transition elements still is not clear, this process makes the optical resistivity at the blackbody centroid larger than the dc value so that a calculation of  $\epsilon_H(\rho_{op}, T)$  in the Mott–Zener regime ( $\langle\omega\rangle\langle 1/\tau\rangle^{-1} > 1$ ) that uses  $\rho_{op}$  instead of  $\rho_{dc}$  provides, in principle, a more realistic comparison with experiment. However, until the source of the high-temperature knee in  $\epsilon_H$  is identified in detail, the predictive value of a correct emissivity calculation for high-temperature transition elements remains in an unsatisfactory state.

## ACKNOWLEDGMENTS

This research is supported by the National Science Foundation under grant DMR-84-09823. Additional support has been received from the Materials Science Center at Cornell University, Materials Science Center Rep. No. 5850.

\* Present address, Department of Engineering Thermophysics, University of Science and Technology of China, Hefei, Anhui, China.

† Present address, Polymer Physics Group, Jet Propulsion Laboratory, California Institute of Technology, 4800 Oak Grove Drive, Pasadena, California 91109.

## REFERENCES

1. A. J. Sievers, "Thermal radiation from metal surfaces," *J. Opt. Soc. Am.* **68**, 1505–1516 (1978).
2. A. J. Sievers, "The emissivity of metals," in *Solar Materials Science*, L. E. Murr, ed. (Academic, New York, 1980), pp. 229–254.
3. C. Davisson and J. R. Weeks, "The relation between the total thermal emissive power of a metal and its electrical resistivity," *J. Opt. Soc. Am.* **8**, 581–605 (1924).
4. W. J. Parker and G. L. Abbott, "Theoretical and experimental studies of the total emittance of metals," in *Symposium on Thermal Radiation of Solids*, S. Katzoff, ed., NASA SP-55 (U.S. Government Printing Office, Washington, D.C., 1965), pp. 11–28.
5. See, for example, Y. S. Touloukian, ed., *Thermophysical Properties of Matter* (Plenum, New York, 1970), Vol. 7.
6. L. A. Wojcik, A. J. Sievers, G. W. Graham, and T. N. Rhodin, "Total hemispherical emissivity of W(100)," *J. Opt. Soc. Am.* **70**, 443–450 (1980).

7. L. A. Wojcik, A. J. Sievers, G. W. Graham, and T. N. Rhodin, "Adsorbate-induced change in the total hemispherical emissivity of W(100)," *J. Opt. Soc. Am.* **72**, 149-155 (1982).
8. R. Smalley and A. J. Sievers, "The total hemispherical emissivity of copper," *J. Opt. Soc. Am.* **68**, 1516-1518 (1978).
9. M. A. Ordal, R. J. Bell, R. W. Alexander, L. L. Long, and M. R. Querry, "Optical properties of fourteen metals in the infrared and far infrared: Al, Co, Cu, Au, Fe, Pb, Mo, Ni, Pd, Pt, Ag, Ti, V, and W," *Appl. Opt.* **24**, 4493-4499 (1985).
10. J. H. Weaver, C. Krafka, D. W. Lynch, and E. E. Koch, *Physics Data, Optical Properties of Metals, Part I: The Transition Metals* (Fachinformationszentrum, Karlsruhe, Federal Republic of Germany, 1981).
11. J. J. Hopfield, "Infrared properties of transition metals," *AIP Conf. Proc.* **4**, 358-366 (1972).
12. S. R. Nagel and S. E. Schnatterly, "Frequency dependence of the Drude relaxation time in metal films," *Phys. Rev. B* **9**, 1299-1303 (1974).
13. D. M. Riffe, L. M. Hanssen, and A. J. Sievers, "Surface-reconstruction-induced changes in free-carrier scattering from the W(100) surface: an infrared surface-electromagnetic-wave study," *Phys. Rev. B* **34**, 692-703 (1986).
14. L. M. Hanssen, D. M. Riffe, and A. J. Sievers, "Infrared surface wave interferometry on W(100)," *Opt. Lett.* **11**, 782 (1986).
15. G. R. Parkins, W. E. Lawrence, and R. W. Christy, "Intraband optical conductivity of Cu, Ag and Au: contribution from electron-electron scattering," *Phys. Rev. B* **23**, 6408-6416 (1981).
16. R. C. Weast, ed., *CRC Handbook of Chemistry and Physics*, 65th ed. (CRC, Boca Raton, Fla., 1984), p. E-381.